Technical Paper

ISSN 1997-1400 Int. J. Pavement Res. Technol. 2(5):188-195

Numerical Modeling of a Roller Compacted Concrete Pavement under Vehicular Loading

Mustapha Zdiri[1,2+], Nor-edine Abriak[2], Mongi Ben Ouezdou[3], Amara Loulizi[4], and Jamel Neji[4]

Abstract: The main objective of pavement design is to calculate the optimal thicknesses of its different structural layers. Therefore the design of rigid pavements, where the rigid slab takes most of the load-carrying capacity, consists on determining the right thickness of the slab. Roller compacted concrete (RCC) pavements, which belong to the family of rigid pavements, are mainly designed and analyzed using existing methods used for jointed plain concrete pavements. These methods are primarily based on Westergaard analytical solution, which determines the mechanical response of a concrete slab under vehicular loading based on many simplifying assumptions. In this study, a 3D numerical model of an RCC pavement was developed using the finite element (FE) software package, ABAQUS. The model treats several aspects that cannot be treated using available analytical solutions. In fact the model treats the base layer and the supporting subgrade as solid elements; friction coefficients are used to simulate the real contact at the interfaces; and the concrete material is modeled using a non-linear behavior law. The modeled pavement was analyzed under a single tire load of 60*kN* with a tire pressure of 740*kPa* applied at three different locations, namely the pavement center, the pavement edge, and the pavement corner. Results of the 3D FE model were compared with those obtained using other methods such as Closed-form Formulas and the Portland Cement Association (PCA) procedure. The comparison showed that the FE model gives lower calculated stresses and higher calculated displacements. It is concluded that 3D FE modeling is a reliable method for the calculation of stresses and displacements in RCC pavements.

Key words: *3D modeling; Displacement; Roller compacted concrete (RCC); Slab loading; Stress.*

Introduction

Roller compacted concrete (RCC) is the commercial name used for concrete placed with conventional hot-mix asphalt paving equipment, then compacted with rollers. The same basic ingredients (water, cement, and aggregates) used to formulate conventional concrete are used to make RCC. However, unlike conventional concrete, RCC is a drier mix made with lower water to cement (w/c) ratio, but with the same cement content. This early stiffness makes the compaction process of RCC a feasible construction method and therefore eliminates the need for forms, finishing, dowels, and steel reinforcement. These properties make the construction of RCC pavements simple, fast, and economical. In addition, the high rigidity of RCC pavements eliminates permanent deformation problems such as rutting and corrugations traditionally encountered in flexible pavements.

Several design methods for rigid pavements were developed over the years by various researchers and institutions in order to determine the necessary concrete slab thickness [1]. Determination of the pavement response to vehicular loadings evolved also over time from using simple closed-form formulas, to the use of influence charts, to the use of finite element (FE) method. Several computer programs to analyze rigid pavements were established based on the FE method including ILLI-SLAB [2], WESLIQID [3], J-SLAB [4], FEACONS-IV [5], ISLAB2000 [6], and WESLAYER [7]. The FE technique have gained widespread use given the recent improvements in computer processing technology and its capability to treat several problems that could not be solved analytically such as load transfer at the joints, dynamic loading, nonlinear material behavior, crack propagation, and many others. In this area and using ABAQUS software, Zaghloul et al. [8], Uddin et al. [9], and Darter et al. [10] developed models for the study of rigid pavements and its foundation.

In the present study, a 3D numerical model of an RCC pavement was developed using the FE software package, "ABAQUS 6.7". The model considers two RCC slabs separated by a joint and laid over a crushed aggregate base over the original subgrade. The main goal of this study is to understand the distribution of the stresses and the displacements in the entire RCC slabs due to a single tire load applied at different locations (middle, edge, and corner) and to compare the results of the FE model with those obtained using other methods.

Application of Existing 2D Models for the Analysis of RCC Pavements

Analysis of rigid pavements consists on determining the stresses, strains, and displacements in the slab induced by vehicular and/or environmental loadings [11]. The first theoretical solutions to the problem of a tire load on a concrete slab laid over a supporting subgrade were proposed by Westergaard in the 1920s [12]. Westergaard's solutions were further developed over the years by

[1] Doctor, Civil Engineering Laboratory, National Engineering School of Tunis, BP 37, Tunis-Belvédère 1002, Tunisia.

[2] Professor, Laboratoire Génie Civil et Environnemental – Ecole des Mines de Douai , Rue Charles Boursel, B.P. 838-59508, France.

[3] Professor, Civil Engineering Laboratory, National Engineering School of Tunis, BP 37, Tunis-Belvédère 1002, Tunisia.

[4] Associate Professor, Applied Mechanics and Systems Research Laboratory - Polytechnic School of Tunis, Tunisia.

[+] Corresponding Author: E-mail zdiri_ms@yahoo.fr

Note: Submitted December 16, 2008; Revised June 4, 2009; Accepted June 26, 2009.

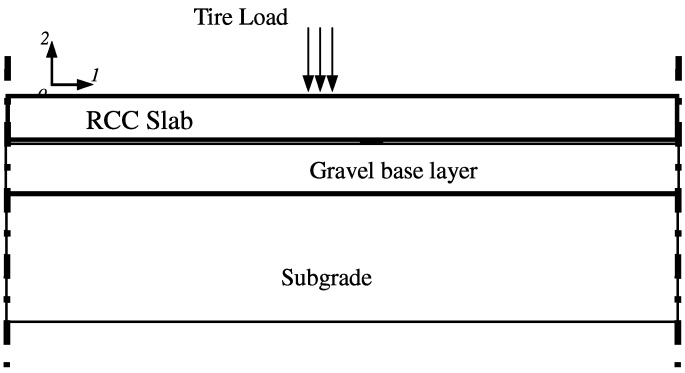

Fig. 1. 2D Model Adopted for a RCC Pavement under a Tire Load.

other researchers and more closed-form formulas and influence charts [13] were suggested to treat the 2D problem shown in Fig. 1.

Corner Loading

For the corner case, Westergaard [12] proposed Eqs. (1) and (2) to calculate the tensile stress σ, and the vertical displacement, Δ, on the bottom surface of the slab, respectively [7].

$$\sigma = \frac{3P}{h^2}\left[1-\left(\frac{a\sqrt{2}}{\ell}\right)^{0.6}\right] \quad (1)$$

$$\Delta = \frac{P}{k\ell^2}\left[1.1-0.88\left(\frac{a\sqrt{2}}{\ell}\right)\right] \quad (2)$$

Where ℓ is the radius of relative stiffness (m) and is expressed by Eq. (3), a is the contact radius (m), P is the concentrated load (N), h is the thickness of the RCC slab (m), and k is the modulus of subgrade reaction (MPa/m).

$$\ell = \left[\frac{Eh^3}{12(1-\nu^2)k}\right]^{0.25} \quad (3)$$

Where E is the elastic modulus of the RCC slab and ν is Poisson's ratio. Ioannides et al. [14] modified the equations proposed by Westergaard and suggested the use of Eqs. (4) and (5) instead.

$$\sigma = \frac{3P}{h^2}\left[1-\left(\frac{c}{\ell}\right)^{0.72}\right] \quad (4)$$

$$\Delta = \frac{P}{k\ell^2}\left[1.205-0.69\left(\frac{c}{\ell}\right)\right] \quad (5)$$

Where $c = 1.77\times a$

To compare between the different presented equations and later on with the FE results, a tire load P = 65,000N with a tire pressure of 740,000Pa, a slab thickness h = 0.20m, and three cases for the modulus of subgrade reaction were treated (k = 30, 90, and 260 MPa/m). Table 1 summarizes the results for these three treated cases.

Interior Loading

For the interior case, Westergaard [12] proposed Eqs. (6) and (7) to calculate the tensile stress, σ, and the vertical displacement, Δ, on the bottom surface of the slab, respectively [7].

$$\sigma = \frac{3(1+\nu)P}{2\pi h^2}\left(Ln\frac{\ell}{b}+0.6159\right) \quad (6)$$

$$\Delta = \frac{P}{8k\ell^2}\left\{1+\frac{1}{2\pi}\left[Ln\left(\frac{a}{2\ell}\right)-0.673\right]\left(\frac{a}{\ell}\right)^2\right\} \quad (7)$$

with $b = a$ if $a \geq 1.724h$

$$b = \sqrt{1.6a^2+h^2}-0.675h \quad \text{if } a < 1.724h$$

The Portland Cement Association (PCA) adopted Eq. (8) in their procedure of design "Design of airport concrete pavement". It leads to calculate the tensile stress in the bottom fiber of the pavement in the slab centre caused by the load of a given axle [1, 15].

$$\sigma = \frac{0.316P}{h^2}\left(4\log\left(\frac{\ell}{b}\right)+1.069\right) \quad (8)$$

Eqs. (6), (7), and (8) were used with the three treated cases. The results are summarized in Table 2.

Table 1. Stresses and Displacements for the Corner Loading Case Using Westergaard and Ioannides Equations.

$E_{Foundation}$	(MPa)	30	150	500
CBR*		5	30	90
E_{RCC}	(MPa)	30,000	30,000	30,000
k	(MPa/m)	30	90	260
ℓ	(m)	0.91	0.70	0.53
σ Westergaard	(MPa)	2.66	2.26	1.80
σ Ioannides	(MPa)	2.643	2.173	1.570
Δ Westergaard	(mm)	2.252	1.162	0.613
Δ Ioannides	(mm)	2.537	1.325	0.713

*CBR: Californian Bearing Ratio.

Table 2. Stresses and Displacements for the Interior Loading Case Using Westergaard and PCA Equations.

$E_{Foundation}$	(MPa)	30	150	500
a	(m)	0.175	0.175	0.175
b	(m)	0.163	0.163	0.163
E_{RCC}	(MPa)	30,000	30,000	30,000
k	(MPa/m)	30	90	260
ℓ	(m)	0.91	0.70	0.53
σ Westergaard	(MPa)	2.222	1.940	1.780
σ PCA	(MPa)	2.083	1.850	1.601
Δ Westergaard	(mm)	0.318	0.182	0.105

Interpretation

For all the studied cases, the calculated displacements for the interior loading case were found to be lower than those calculated for the corner loading case. Moreover, the obtained stresses due to interior loading were 85% of that due to corner loading however the deflections were only about 15%. This is only true when there is no load transfer by the joints at the corner. In the case of load transfer

Table 3. Stresses and Displacements for the Edge Loading Case Using Westergaard and ALIZE Equations.

$E_{Foundation}$	(*MPa*)	30	150	500
a	(*m*)	0.175	0.175	0.175
b	(*m*)	0.163	0.163	0.163
E_{RCC}	(*MPa*)	30,000	30,000	30,000
k	(*MPa/m*)	30	90	260
ℓ	(*m*)	0.91	0.70	0.53
σ Westergaard	(*MPa*)	3.9	3.3	2.7
σ ALIZE	(*MPa*)	3.11	2.687	2.238
Δ Westergaard	(*mm*)	1.292	0.702	0.376

by the joints at the corners the stresses due to corner loading will be lower than that due to interior loading whereas the displacements remain without variations and this is in analogy with the ideas developed by Huang Yang [7, 16].

Edge Loading

For the edge case, Westergaard [12] proposed Eqs. (9) and (10) to calculate the tensile stress, and the vertical displacement on the bottom surface. These equations represent the solutions for the maximum stresses σ and displacement Δ produced by loads applied in the edges of a rigid slab [7]. They were modified after that by Ioannides et al. [14], to be presented in the following forms:

$$\sigma=\frac{3(1+\nu)P}{\pi(3+\nu)h^2}\left[Ln\left(\frac{Eh^3}{100ka^4}\right)+1.84-\frac{4\nu}{3}+\frac{1-\nu}{2}+\frac{1.18(1+2\nu)a}{\ell}\right] \quad (9)$$

$$\Delta=\frac{\sqrt{2+1.2\nu}P}{\sqrt{Eh^3k}}\left[1-\frac{(0.76+0.4\nu)a}{l}\right] \quad (10)$$

In the French mechanistic-empirical procedure to design pavements (programmed in the ALIZE software), the maximum tensile stress at the bottom fibers at the edge of the slab is calculated using Eq. (11) [17].

$$\sigma=\frac{0.572P}{h^2}(4\log\left(\frac{\ell}{b}\right)+0.359) \quad (11)$$

Eqs. (9), (10), and (11) were used with the three treated cases. The results are summarized in Table 3.

Interpretation

The results for all the studied cases show that the calculated stresses for the edge loading case were higher than those calculated for the interior and corner loading cases. On the other hand, the calculated displacements for the edge loading case are smaller than those calculated for the interior and corner loading cases.

Application of the Dantu Method to Analyze RCC Pavements

Dantu analyzed the maximum stresses in a slab of limited size made of an elastic material (cork) by measuring deformation induced by a load applied at different locations using optical sensors [18]. Equations of the moments M as function of Z are defined by Eqs. (12) through (15).

Table 4. Stresses for Three Treated Cases Using Dantu's Equations.

$E_{Foundation}$	(*MPa*)	30	150	500
a	(*m*)	0.175	0.175	0.175
k	(*MPa/m*)	30	90	260
ℓ	(*m*)	0.91	0.70	0.53
Z		0.16	0.28	0.42
σ (Interior)	(*MPa*)	2.14	1.71	1.38
σ (Edge)	(*MPa*)	4.54	3.254	2.27
σ (Corner)	(*MPa*)	1.81	1.174	0.644

- Interior loading case:

$$M = P(1+\nu)\frac{1}{3.60+12\times Z} \quad (12)$$

- Edge loading case:

$$M = P(1+\nu)\frac{1}{1.70+4.1\times Z+10.3\times Z^2} \quad (13)$$

with

$$Z = \frac{a}{h}\sqrt[3]{6\frac{E_f\left(1-\nu^2\right)}{E\left(1-\nu_f{}^2\right)}} \quad (14)$$

- Corner loading case where the moment is maximum:

$$M = P(1+\nu)\frac{1}{7-21\times Z+115\times Z^2} \quad (15)$$

The stresses are calculated by dividing the moments with the sections modulus as shown by Eq. (16).

$$\sigma = \frac{6M}{b\times h^2} \quad (16)$$

Dantu's equations were used to find the stresses for the three treated cases and the results are presented in Table 4.

Interpretation

Values of moments and stresses were found higher in the edge loading case than in the other loading cases.

Three Dimensions Numerical Model by the FE Software Package "Abaqus 6.7"

The 3D Modeling Objectives

All previously presented formulas are very simple to use, but are based on many simplifying assumptions. In fact, the models consider only two layers in two dimensions, the two layers are perfectly bonded, the concrete is considered as a linear elastic material, and the subgrade cannot transmit shear stresses. All the analytical solutions of the 2D models were based on the proposal that the slab and the foundation were in perfect contact [18]. For these reasons, a 3D numerical modeling of the RCC slab was used by introducing, to the computer code "Abaqus 6.7" [19], the behavior law of the RCC. The present method of calculation by

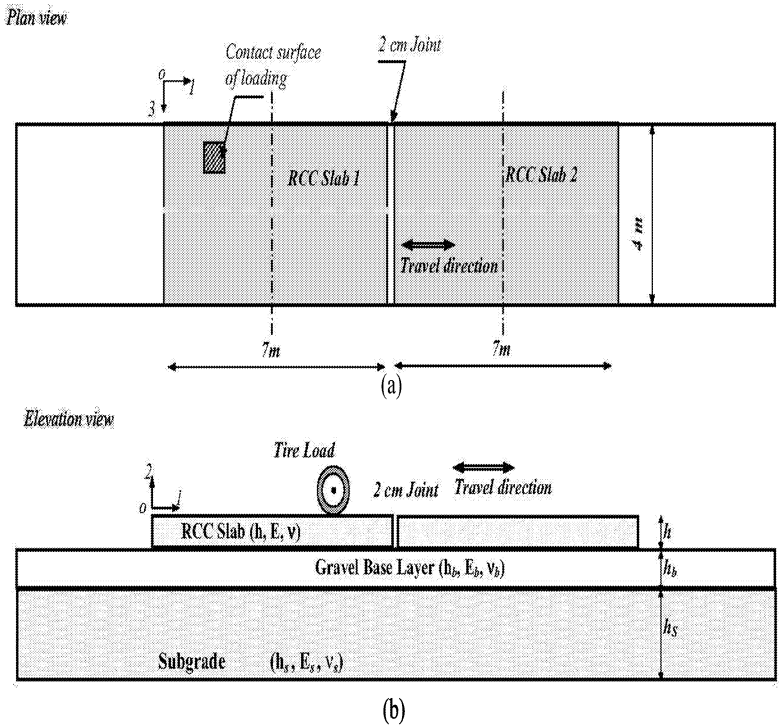

Fig. 2. Model Adopted for the RCC (a) Plan and (b) Elevation View.

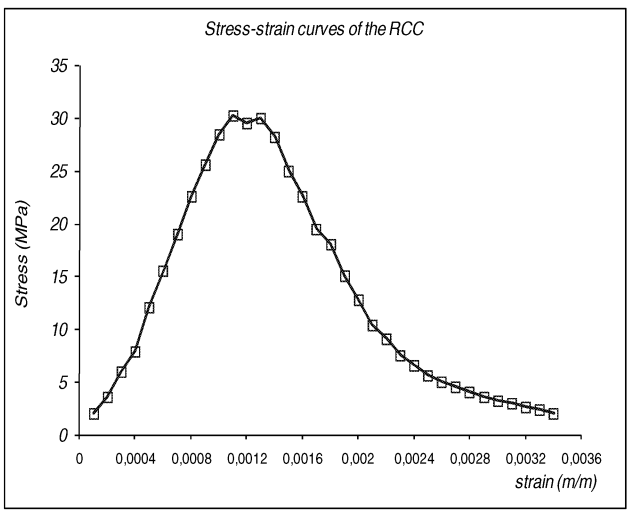

Fig. 3. Representation of the RCC Stress-Strain Relation.

finite elements allows the transformation of the continuous problem into a discrete problem. The solution obtained is approximate according to the model data. In the proposed model, a solid foundation was used, which is more realistic although this modeling requires much more memory for the resolution. The solid foundation is more realistic than the liquid foundation, because the displacement in any nodal point depends not only on the force in this node but also on the forces in all the other nodes. With the advantages of calculations of the numerical methods by computers, the developed analyses were based on a partial contact between the layers [7].

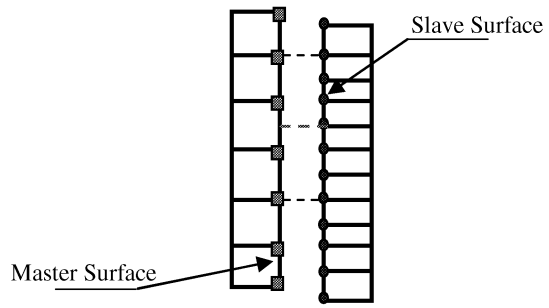

Fig. 4. Contact Graph and Surfaces Interactions.

The aims through this numerical approach were the use of the numerical computer code Abaqus 6.7 for 3D modeling of the RCC pavement and the study of the distribution and the evolution of the stresses and the strains in a RCC slabs. The results were shown especially for many loading position, in top and bottom fibers and in the interface with the sub-base.

Description of the Numerical 3D Model

The modeled pavement structure, shown in Fig. 2, consists of two RCC slabs separated by a 2-cm-joint placed over a crushed gravel base and the original subgrade [20]. All the modeled elements are finite in the three dimensions. The crushed aggregate was treated as a linear elastic material. The subgrade was also treated as homogeneous and with linear elastic behavior. A solid foundation was used in the model because it is more realistic than the liquid

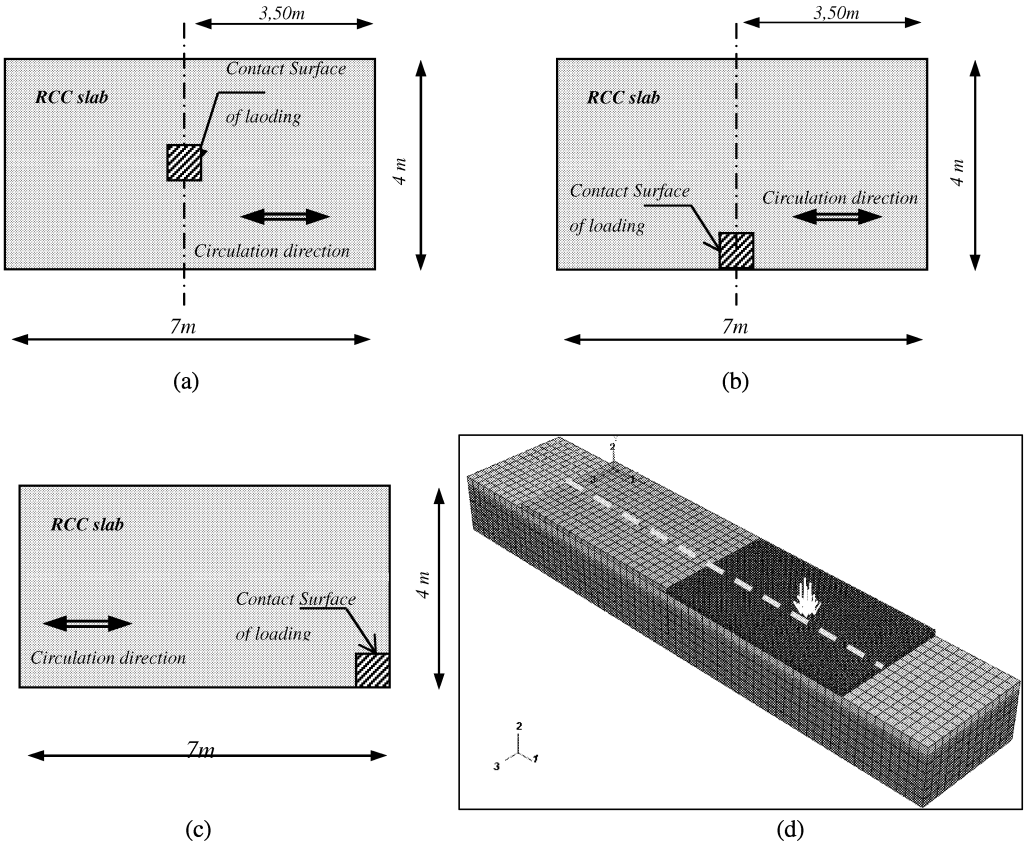

Fig. 5. Different Treated Loading Cases (a) Interior Loading Case, (b) Edge Loading Case, (c) Corner Loading Case, and (d) 3D Model for the Interior Loading Case.

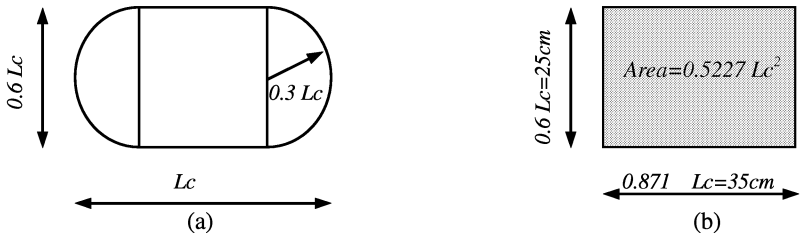

Fig. 6. The Adopted Contact Surface of Tire (a) Real Tire Contact Surface and (b) Equivalent Tire Contact Surface.

foundation even though it requires much more computational time. Friction coefficients were used to simulate the bonding at the different interfaces. The thicknesses of the RCC slab, the base, and the subgrade were fixed in three dimensions. The different input parameters for the model are as follows:

- Two RCC slabs of ($4.00 \times 7.00m$), $h = 20cm$, $E = 30{,}000MPa$, $\nu = 0.22$.
- Crushed gravel base layer of ($4.00 \times 20.00m$), $h_b = 30cm$, $E_b = 150MPa$, $\nu_b = 0.35$.
- Subgrade of ($4.00 \times 20.00m$), $h_s = 120cm$, $E_s = 50MPa$, $\nu_s = 0.45$.
- The slab/base layer friction ratio = 1.5; the base/subgrade friction ratio = 1.1.

The temperature differential between the top and bottom RCC slab is assumed to be equal to 11°C [21]. The RCC slab length of $7m$ was chosen since it represents an average value for reported slab lengths in the literature (4.5 to $9.2m$) [3, 5].

RCC Mechanical Behavior

To suitably simulate the mechanical behavior of RCC in compression, an experimental behavior law as presented by Fig. 3 was introduced into the finite elements code. The RCC behavior in tension was supposed to be linear elastic until a stress that represents the beginning of RCC cracking. After this stress, RCC develops a linear loss of resistance behavior [19].

Meshing and Boundary Conditions

The boundary conditions were selected in order to approach as much as possible to the actual situation. The gravel sub-base was fixed in the two directions 1 and 3; however the ground support layer was fixed in the two directions 1 and 2. The two RCC slabs were fixed on one face in directions 1 and 2. The gravel sub-base

Table 5. Stresses in RCC Slab as Obtained with the FE Model (Contact with Friction Ratio).

Stress (*MPa*)	Interior Loading Case		Corner Loading Case		Edge Loading Case	
	Top Fibers	Bottom Fibers	Top Fibers	Bottom Fibers	Top Fibers	Bottom Fibers
σ_{11}	1.670	1.470	2.090	1.406	2.330	1.740
σ_{22}	0.791	0.280	0.755	0.299	0.675	0.328
σ_{33}	1.649	1.482	1.057	1.405	0.613	0.379
σ_{12}	0.249	0.249	0.682	0.682	0.529	0.529
σ_{13}	0.210	0.210	0.938	1.044	0.758	0.840
σ_{23}	0.250	0.250	0.232	0.232	0.315	0. 315

and the two slabs were free in direction 2 and they can move in this direction. Only, the ground support was fixed in the direction 3 (Figs. 1 and 2). Meshes based on hexahedrons with eight nodes were chosen. The size of the meshes was also optimized in order to obtain a compromise between the computational time and the stability of calculation (Fig. 4). It was found that a fine mesh (10 by 10*cm*) is required in the RCC slab supporting the load. However a relatively coarser mesh (30 by 30*cm*) was chosen in the gravel sub-base, ground support, and RCC slab not supporting the load. It did not significantly affect the precision of the stress and displacement prediction.

In the present study, the assumptions considered in this modeling, consists of a friction ratio between the RCC slab and the gravel foundation. Another friction ratio between the sub-base and the support ground was taken into consideration.

Various Cases of Loadings

As shown in Fig. 5, three loading cases were analyzed using the FE model: interior loading case, edge loading case, and corner loading case. The applied load magnitude (65,000*N*) and tire pressure (740,000*Pa*) were similar to the values used in the cases treated using the previously discussed 2D models in order to be able to compare between the FE results and the other methods.

In their studies, ARA and ERES [21] reported that load transfer efficiency (LTE) at the transverse joints has only a limited effect on the distribution of the RCC bottom surface stresses. For this reason, this property was not taken into account in the present model.

To assure adequate simulation of the tire-pavement contact area, tire footprints were modeled using rectangular shapes with equivalent contact areas as showed in Fig. 6.

FE Model Results

In order to well-exploit the output of the FE 3D model, the values of the stresses and displacements in the loading position and in the interfaces were extracted, whereas the stress and displacement distributions in other parts of the RCC slab, the base layer, and the subgrade were schematized in the form of color curves as presented in Figs. 7 to 12.

Stress Distributions

Table 5 presents the six-components of the stress as obtained with the 3D FE model at different locations in the RCC slab for the three loading cases. Figs. 7 to 9 show the distribution of the longitudinal horizontal stress (σ_{11}) in the RCC slab for the interior loading case.

As expected, the maximum values of the stresses and the strains were found on the top fibers (compression) and bottom fibers (tension) of the RCC slab. The maximum values of the stresses were in direction 1 (longitudinal) and were found for the edge loading case. Maximum shear stresses were n the 1-3 plane with the highest value of 1.04*MPa* calculated for the corner loading case.

Displacements

Table 6 shows the calculated displacements using the FE model in the RCC slab for the different loading cases. The distributions of the vertical displacement in the RCC slab, the base layer, and the subgrade are schematized by graphs presented in Figs. 10 to 12. In all loading cases, displacements in direction 2 were higher compared to those in direction 1 and 3. In this vertical direction, the maximum displacement in the corner loading case (1.84*mm*) was higher than those in the other loading cases (0.40*mm* for the interior loading case and 1.25*mm* for the edge loading case).

Table 6. Displacements in RCC Slab as Obtained with the FE Model.

Displacement (*m*)	Corner Loading Case		Interior Loading Case		Edgel Loading Case	
	Top Fibers	Bottom Fibers	Top Fibers	Bottom Fibers	Top Fibers	Bottom Fibers
Δ_1	3.75×10^{-5}	3.34×10^{-5}	2.67×10^{-5}	2.67×10^{-5}	6.43×10^{-5}	6.43×10^{-5}
Δ_2	1.84×10^{-3}	1.84×10^{-3}	0.40×10^{-3}	0.40×10^{-3}	1.25×10^{-3}	1.25×10^{-3}
Δ_3	1.43×10^{-4}	1.72×10^{-4}	3.04×10^{-5}	3.04×10^{-5}	1.24×10^{-4}	4.06×10^{-5}

Table 7. Results of the Stresses and Displacements for Three Loading Cases by Different Methods.

Methods	Corner Loading		Interior Loading (Centre)		Edge Loading	
	Stress (*MPa*)	Displacement (*mm*)	Stress (*MPa*)	Displacement (*mm*)	Stress (*MPa*)	Displacement (*mm*)
Westergaard	2.26	1.162	1.940	0.182	3.30	0.702
Ioannides et al.	2.173	1.325	-	-	-	-
PCA	-	-	1.850	-	-	-
ALIZE	-	-	-	-	2.687	-
Dantu	1.174	-	1.71	-	3.254	-
FE model	1.406	1.84	1.470	0.40	1.740	1.25

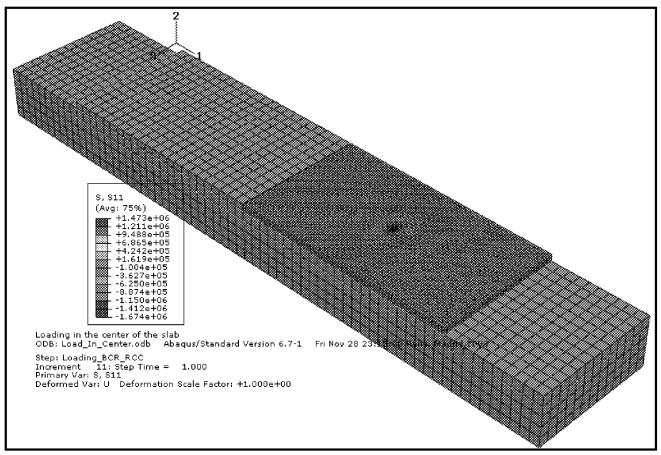

Fig. 7. Stress Distribution in Top Fibers for the Interior Loading Case.

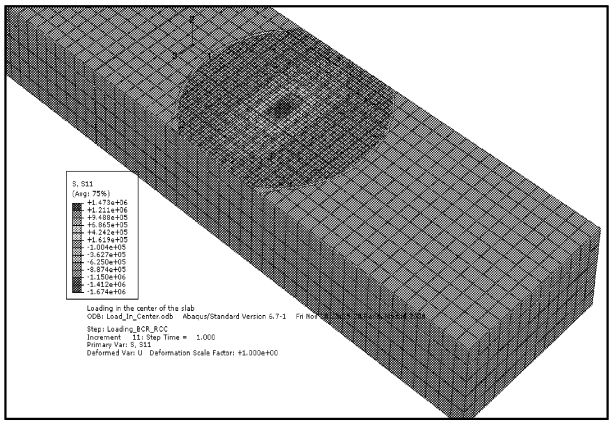

Fig. 8. Stress Distribution in Bottom Fibers for the Interior Loading (Contact with Friction Ratio).

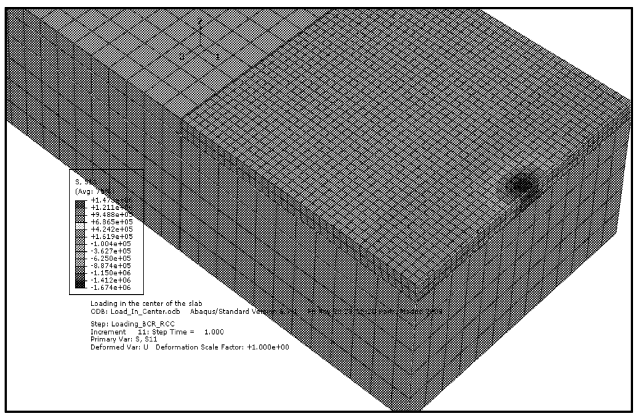

Fig. 9. Stress Distribution in Top and Bottom Fibers for the Interior Loading Case.

Comparison and Interpretation of the Results of the Various Methods

RCC pavements belong to the family of rigid pavements where the slab bends elastically under the loads. It distributes the stresses on a large area to the supporting subgrade. This principle was visualized by the graphic distribution of stresses in the 2-direction where at the subgrade level the stresses were found to be generally very low.

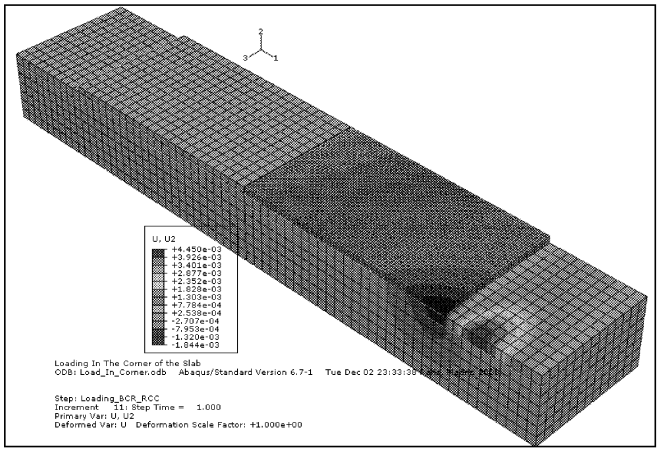

Fig. 10. Distribution of Vertical Displacements for the Corner Loading Case.

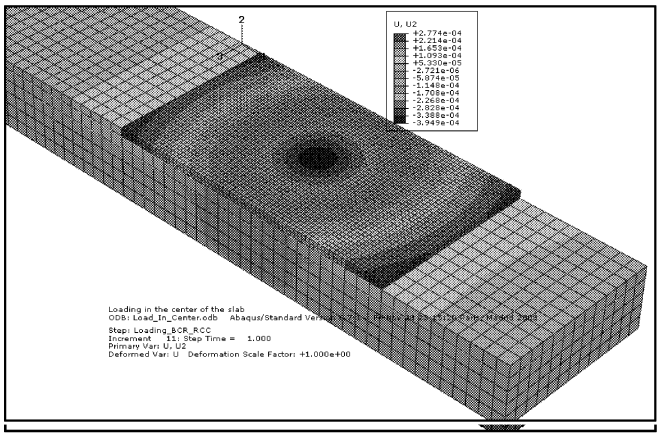

Fig. 11. Distribution of Vertical Displacements for the Interior Loading Case.

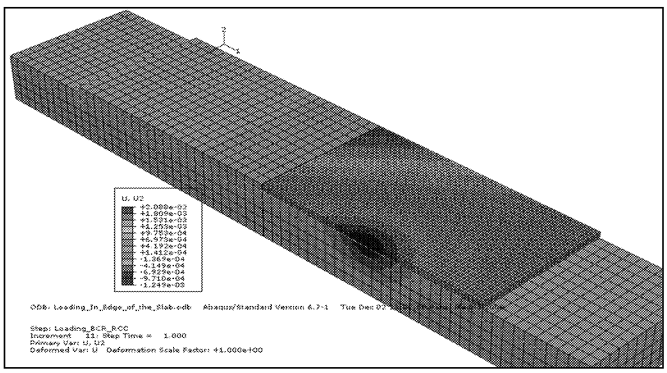

Fig. 12. Distribution of Vertical Displacements for the Edge Loading Case.

Table 7 presents a comparison between the calculated responses using the 3D FE model and the available analytical solutions presented earlier in the paper. For the corner loading case, the methods of Westergaard and Ioannides et al. gave very similar stress results. The FE model gave lower stress, but higher displacements than the other methods. Results using Dantu's method were in generally different from those given by all others methods. In the interior loading case, the methods of Westergaard and PCA gave very close stress results. For the edge loading case, the methods of

Westergaard, Ioannides et al., and Dantu gave very close stress results.

Conclusions

Through the present study, the following conclusions are drawn:

- The comparisons of the stresses and displacements predicted by several 2D methods with those obtained using the 3D FE model showed some correspondences although the FE results were lower in stresses and higher in displacements.
- All methods used with all cases analyzed show that the edge loading case induces higher stresses then interior and corner loading cases
- As presented by many other researchers, this work confirmed that the use of FE is a powerful tool for 3D modeling of RCC pavements. The main particularity of this study is the introduction of the special mechanical behavior law for the RCC material.

References

1. Gauthier, P. and Marchand, J., (2004). Conception et réalisation de revêtements en béton compacté au rouleau au Québec, *Association Béton, Québec (ABQ)*, Québec, pp. 63-87.
2. Tabatabaie, A.M. and Barenberg, E.J., (1980). Structural Analysis of Concrete Pavement Systems, *Journal of Transportation Engineering*, ASCE, National Research Council, Washington, DC, 106(5), pp. 493-506.
3. Chou, Y.T., (1981). Structural Analysis Computer Programs for Rigid Multicomponent Pavement Structures with Discontinuities: WESLIQUID and WESLAYER, *Technical Report GL-81-6*, U.S. Army Engineer Waterways Experiment Station, Vicksburg, MS, USA.
4. Tayabji, S.D. and Colley, B.E., (1986). Analysis of Jointed Concrete Pavements, *Report No. FHWA/RD-86/041*, Federal Highway Administration, McClean, VA, USA.
5. Choubane, B. and Tia, M., (1995). Analysis and Verification of Thermal-Gradient Effects on Concrete Pavement, *Journal of Transportation Engineering*, 121(1), pp. 75-81.
6. Khazanovich, L., Yu, H.T., Rao, S., Galasova, K., Shats, E., and Jones, R., (2000). ISLAB2000, Finite Element Analysis Program for Rigid and Composite Pavements, *User's Guide*, ERES Consultants, Champaign, Illinois, USA.
7. Huang, Y. H., (2004). *Pavement Analysis and Design*, 2nd Edition, Prentice Hall, pp. 147-166, University of Kentucky, USA.
8. Zaghloul, S.M., White, T.D., Vincent, P.D., and Drian, C., (1994). Dynamic Analysis of FWD and Pavement Response Using a Three-Dimensional Dynamic Finite Element Program, *Nondestructive Testing of Pavements and Back calculation of Modulus (2nd Volume), ASTM STP 1198*, American Society for Testing and Materials, Philadelphia, PA, USA.
9. Uddin, W., Noppakunwijai, P., and Chung, T., (1997). Performance Evaluation of Jointed Concrete Pavement Using Three-Dimensional Finite-Element Dynamic Analysis, *the 76th Transportation Research Board Annual Meeting*, Paper No. 1414, Transportation Research Board of the National Academies, Washington, DC, USA.
10. Darter, M., Khazanovich, L., Snyder, M., Rao, S., and Hallin, J., (2001). Development and Calibration of a Mechanistic Design Procedure for Jointed Plain Concrete Pavements. *Proceedings, 7th International Conference on Concrete Pavements*, Orlando, FL, USA.
11. Patricio, T.M., Wasantha, K., Mang, T., Wu, C.L., and Choubane, B., (2008). Evaluation of Composite Pavements Using a Heavy Vehicle Simulator, *International Journal of Pavement Research and Technology*, 1(1), pp. 1-11.
12. Westergaard, H.M., (1926). Stress in Concrete Pavement Computed by Theoretical Analysis, *Publics Roads*, 7(2), pp. 25-35.
13. Pickett's, G. and Ray, G.K., (1951). Influence Chart for Concrete Pavement, *Transactions, ASCE*, Vol. 116, pp 49-73.
14. Ioannides, A.M., Thompson, M.R., and Barenberg, E.J., (1985). Westergaard Solutions Reconsidered, *Transportation Research Record*, No. 1043, pp. 13-23.
15. Portland Cement Association, (2004). *Guide Specification for Construction of Roller-Compacted Concrete Pavements*, IS009.01, 8p. Portland Cement Association, USA.
16. Chiu, L., Zhongren, W., and James, N.L., (2008). Influence of Concrete Joints on Roughness Index and Pavement Serviceability, *International Journal of Pavement Research and Technology*, 1(4), pp. 143-147.
17. Jeuffroy, G. and Sauterey, R., (1989). *Cours de routes, Chaussée en béton de ciment*, pp. 49-79, Presse de l'Ecole Nationale des Ponts et chausses, Paris, France.
18. Coquand, R., (1989). *Routes, Chaussées rigides et chaussées souples*, 8eme Edition, Eyrolles, Paris, France.
19. Abaqus guide Version 6.7, (2007). Computer Software for Interactive Finite Element Analysis, *Abaqus guide Version 6.7*, Hibbitt, Karlsson & Sorensen, Inc. Pawtucket, RI, USA.
20. Chou, C.P. and Lee, M.H., (2008). Analysis of Slab Thermal Stresses and Concrete Joint Movements, *International Journal of Pavement Research and Technology*, 1(4), pp. 148-154.
21. ARA, Inc., ERES Division, (2003). Guide for Mechanistic-Empirical Design of New and Rehabilitated Pavement Structures, *NCHRP Project 1-37A*, ARA, Inc., ERES Division, USA.

.